

Accuracy of Spencer-Attix cavity theory and calculations of fluence correction factors for the air kerma formalism

D. J. La Russa^{a)} and D. W. O. Rogers^{b)}

Ottawa Carleton Institute of Physics, Carleton University Campus, Ottawa, Ontario K1S 5B6, Canada

(Received 23 December 2008; revised 18 June 2009; accepted for publication 19 June 2009; published 12 August 2009)

EGSnrc calculations of ion chamber response and Spencer-Attix (SA) restricted stopping-power ratios are used to test the assumptions of the SA cavity theory and to assess the accuracy of this theory as it applies to the air kerma formalism for ^{60}Co beams. Consistent with previous reports, the EGSnrc calculations show that the SA cavity theory, as it is normally applied, requires a correction for the perturbation of the charged particle fluence (K_{fl}) by the presence of the cavity. The need for K_{fl} corrections arises from the fact that the standard prescription for choosing the low-energy threshold Δ in the SA restricted stopping-power ratio consistently underestimates the values of Δ needed if no perturbation to the fluence is assumed. The use of fluence corrections can be avoided by appropriately choosing Δ , but it is not clear how Δ can be calculated from first principles. Values of Δ required to avoid K_{fl} corrections were found to be consistently higher than Δ values obtained using the conventional approach and are also observed to be dependent on the composition of the wall in addition to the cavity size. Values of K_{fl} have been calculated for many of the graphite-walled ion chambers used by the national metrology institutes around the world and found to be within 0.04% of unity in all cases, with an uncertainty of about 0.02%. © 2009 American Association of Physicists in Medicine. [DOI: 10.1118/1.3174862]

Key words: air kerma, primary standards, Spencer-Attix cavity theory, ^{60}Co , EGSnrc, fluence perturbation correction

I. INTRODUCTION

The equation used by primary standards laboratories to determine the air kerma (K_{air}) in a ^{60}Co beam from measurements of the charge collected by an ion chamber free in air is given by¹

$$K_{\text{air}} = \frac{Q_{\text{gas}}}{m_{\text{air}}(1 - \bar{g}_{\text{air}})} \left(\frac{W}{e} \right)_{\text{air}} \left(\frac{\bar{L}_{\Delta}}{\rho} \right)_{\text{air}}^{\text{wall}} \left(\frac{\bar{\mu}_{\text{en}}}{\rho} \right)_{\text{air}}^{\text{wall}} \times K_h K_{\text{wall}} K_{\text{an}} K_{\text{comp}} K, \quad (1)$$

where $Q_{\text{gas}}/m_{\text{air}}$ is the charge measured in humid air per unit mass of dry air that would occupy the cavity at standard temperature and pressure, $(W/e)_{\text{air}}$ is the mean energy deposited in dry air per unit charge of one sign released, \bar{g}_{air} is the fraction of charged particle kinetic energy lost to radiative processes, $(\bar{\mu}_{\text{en}}/\rho)_{\text{air}}^{\text{wall}}$ is the spectrum-averaged ratio of mass-energy absorption coefficients, and $(\bar{L}_{\Delta}/\rho)_{\text{air}}^{\text{wall}}$ is the Spencer-Attix (SA) ratio of restricted mass-collision stopping powers, often referred to as the stopping-power ratio. The correction factors for humidity (K_h), attenuation and scatter by the wall (K_{wall}), axial nonuniformity of the beam (K_{an}), and material inhomogeneities in the chamber (K_{comp}) have been formally defined elsewhere.²⁻⁴ Accurately determining these correction factors using Monte Carlo methods (except for K_h) has been the topic of many previous investigations. Additional corrections to account for nonideal conditions, such as radial nonuniformity of the beam or electrodes made with a different material, are typically accounted for by K .

In Monte Carlo investigations of the air kerma formalism, the geometry and physics of the simulation can be defined such that the various correction factors discussed above are, by definition, unity.^{3,4} Under these simulation conditions, the accuracy of the air kerma formalism given by Eq. (1) is limited by the accuracy of the SA cavity theory. Recognizing this, Borg *et al.*⁵ introduced a correction factor, K_{SA} , to account for the discrepancy between the response of ion chambers (referred to here as the charge per unit mass per unit incident fluence) and the predictions of the SA cavity theory. They calculated it as a function of energy (from 100 keV to a few MeV) for the graphite chambers used as ^{60}Co air kerma standards at NRC, BIPM, and NIST. Their calculated values of K_{SA} ranged between 0.9970 and 1.0005 for a ^{60}Co beam depending on the chamber and the value of low-energy cutoff Δ used in the calculation of stopping-power ratio. Buckley *et al.*⁶ later showed that K_{SA} is unity for one particular graphite thimble chamber at ^{60}Co energies but is a 0.5% correction (1.0050 ± 0.0003) for the same chamber configured with an aluminum thimble. However, neither study determined whether the K_{SA} correction was due to fluence perturbations by the cavity or due to the wrong choice of Δ in the calculation of the SA stopping-power ratio since, as we discuss in the following sections, this requires an in-depth knowledge of how K_{SA} is affected by changes in chamber wall material and cavity dimension.

In this investigation, the source of the K_{SA} correction is deduced from EGSnrc calculations of $K_{\text{SA}}(\bar{L}_{\Delta}/\rho)_{\text{air}}^{\text{wall}}$ as a function of cavity size for an idealized plane-parallel (pp) ion chamber modeled using a range of wall materials. The ap-

proach to our analysis is outlined following an overview of the SA cavity theory as it is applied to the determination of air kerma.

I.A. Overview of Spencer-Attix cavity theory

The widespread adoption of the Spencer-Attix cavity theory⁷ traces back to the general observation in the 1950s and 1960s that it could account for the variation in response measured as a function of cavity dimension or cavity air pressure for chambers free in air,⁷⁻¹⁰ whereas preceding cavity theories, such as that by Bragg and Gray, could not. In the simplest application, as it was originally applied, the SA cavity theory assumes that for a cavity filled with medium g surrounded by material m and located within an unscattered, unattenuated photon beam, the cavity is small enough such that it does not perturb the fluence of charged particles in medium m , and the dose deposited in medium g is completely due to charged particles originating in medium m . Under these conditions, the ratio of D_m , the dose to medium m , and D_g , the dose to medium g , is equal to the SA stopping-power ratio:¹⁰

$$\frac{D_m}{D_g} = \left(\frac{\bar{L}_\Delta}{\rho} \right)_g^m, \quad (2)$$

where

$$\left(\frac{\bar{L}_\Delta}{\rho} \right)_g^m = \frac{\int_\Delta^{E_{\text{max}}} \Phi_m(E) \left(\frac{L_\Delta(E)}{\rho} \right)_m dE + \Phi_m(\Delta) \left(\frac{S(\Delta)}{\rho} \right)_m \Delta}{\int_\Delta^{E_{\text{max}}} \Phi_m(E) \left(\frac{L_\Delta(E)}{\rho} \right)_g dE + \Phi_m(\Delta) \left(\frac{S(\Delta)}{\rho} \right)_g \Delta} \quad (3)$$

and D_m is the dose to medium at the point of measurement of the cavity, without the cavity present. In Eq. (3), $\Phi_m(E)$ is the fluence of charged particles, including all secondary knock-on electrons (δ rays), with energy E in medium m (i.e., the unperturbed fluence), $(L_\Delta(E)/\rho)_i$ is the mass-collision stopping power at energy E for medium i restricted to collisional energy losses below an energy threshold Δ , and $(S(\Delta)/\rho)_i$ is the unrestricted stopping-power for medium i at $E = \Delta$. The original formulation for $(\bar{L}_\Delta/\rho)_g^m$ did not explicitly include the track-end terms [$\Phi_m(\Delta)(S_i(\Delta)/\rho)\Delta$] since the energy dissipation of electrons with $E \leq \Delta$ was accounted for via a unique evaluation of the restricted stopping powers for $\Delta \leq E \leq 2\Delta$.¹¹ The form of the track-end terms required when conventional restricted stopping powers are used has been derived by Nyström and Nahum.¹²

Applied to ion chambers, m and g represent the wall material and cavity gas, respectively. The cavity gas is assumed to be dry air for the purposes of this discussion so that K_h is unity. Under conditions of charged particle equilibrium, which in principle requires no attenuation or scatter of the incident photon fluence, $D_{\text{wall}} = \Psi(\bar{\mu}_{\text{en}}/\rho)_{\text{wall}}$, where Ψ is the incident parallel photon energy fluence. Inserting this into Eq. (2) and rearranging for D_{air} , we find that for this idealized case

$$D_{\text{air}} = \Psi \left(\frac{\bar{L}_\Delta}{\rho} \right)_{\text{wall}}^{\text{air}} \left(\frac{\bar{\mu}_{\text{en}}}{\rho} \right)_{\text{wall}}. \quad (4)$$

D_{air} is directly proportional to the charge in dry air, Q_{air} . In other words, the response one measures is directly proportional to $(\bar{L}_\Delta/\rho)_{\text{wall}}^{\text{air}}(\bar{\mu}_{\text{en}}/\rho)_{\text{wall}}$. By dividing both sides of Eq. (4) by $K_{\text{air}} = \Psi(\bar{\mu}_{\text{en}}/\rho)_{\text{air}}[1/(1-\bar{g}_{\text{air}})]$ and noting that $D_{\text{air}} = (Q_{\text{air}}/m_{\text{air}})(W/e)_{\text{air}}$, we can obtain the expression for K_{air} given by Eq. (1) without the K_{wall} , K_{an} , and K_{comp} correction factors.

The ability of the SA cavity theory to account for the cavity-size dependence of chamber response, as discussed above, is attributed to the parameter Δ in the stopping-power ratio, introduced by Spencer and Attix to account for the production of δ rays in the fluence of charged particles. Δ is loosely defined as the threshold energy an electron needs to cross the cavity and is often taken as the energy of an electron with a range in air, determined from the continuously slowing down approximation (CSDA), equal to the mean chord length in the cavity, L . For a convex cavity in an isotropic field, L can be shown to be equal to $4V/S$, where V is the cavity volume and S is the surface area of the cavity.^{3,10} Using Monte Carlo simulations, it has been shown that this prescription for L is a particularly good approximation for plane-parallel and Baldwin-Farmer-type chambers in a ^{60}Co beam.³

Using the $4V/S$ approach to determine Δ , SA predicted values of the response can be obtained using Eq. (4) for a variety of chamber wall materials and cavity dimensions. The accuracy of these predictions can be determined via comparisons with some of the classic experiments from the 1950s that were specifically designed to test cavity theory. Two such experiments were performed by Cormack and Johns¹³ in 1954 and by Whyte¹⁴ in 1957. Cormack and Johns¹³ measured the ionization as a function of cavity height (distance between the front and back walls) for a plane-parallel ion chamber configured with several wall materials and compared their results with theoretical predictions based on the Bragg-Gray cavity theory. Whyte's experiment¹⁴ involved the measurement of ionization per unit mass as a function of cavity air pressure for a large cylindrical chamber, which had changeable wall and electrode materials. Changing cavity air pressure is similar to changing the physical cavity dimension since it changes the distance in g/cm^2 that a charged particle must travel to cross the cavity. EGSnrc simulations of these two experiments (as well as others) are discussed in our preceding paper.¹⁵ In general, the calculations of chamber response are within 0.5% for the Whyte chamber and 1.4% for the Cormack and Johns chamber when responses for all wall materials are considered simultaneously. This is comparable to the uncertainties in the cross sections and stopping powers at these energies, as well as the assumed uncertainties on the experimental measurements (see Ref. 15 for additional details). Other experiments of this type were also performed during that time, including the classic experiment by Attix *et al.*⁸ However, those results

are not considered here since many of the important experimental details were not included.

Given the proven ability of EGSnrc to simulate these classic experiments, we can use the calculated results of our previous investigation to test the SA cavity theory. Comparing the theory to Monte Carlo-calculated results ensures that any observed discrepancies are not attributed to uncertainties in cross-section data since a consistent set of cross sections is used in all calculations. As we will show, SA cavity theory is, in general, unable to predict chamber response at the level of accuracy required for primary and secondary standards laboratories although for graphite-walled ion chambers it is remarkably accurate. Following this comparison, a more in-depth analysis of SA cavity theory will be performed using the calculated response of an idealized plane-parallel chamber in order to determine the exact source of its limitations.

II. METHODS

II.A. EGSnrc calculations of chamber response

Following the approach of the original experiments in the 1950s and 1960s, the SA cavity theory is extensively tested via comparisons with EGSnrc-calculated values of chamber response. The CAVRZnrc user code¹⁶ of EGSnrc (Refs. 17 and 18) was used to calculate the response to a ^{60}Co beam of both the Cormack and Johns¹³ and Whyte¹⁴ realistic chambers using models previously described,¹⁵ and an “idealized” pp ion chamber modeled with a variety of wall materials and cavity heights. EGSnrc is known to be well suited for ion chamber calculations, particularly for pp chambers at ^{60}Co energies.^{15,19,20} The idealized chamber was simulated without an insulator or collector (i.e., homogeneous walls), and no guard ring was included. To provide full buildup, the walls were set slightly thicker than the CSDA range of the maximum-energy electrons in the charged particle fluence spectrum. The radius of the cavity was 1.2 cm and was filled with dry air in the simulations. The response of the chamber is directly proportional to the calculated dose per unit incident fluence to the cavity (D_{air}/Ψ), which was calculated using the photon regeneration option¹⁶ with a realistic ^{60}Co spectrum²¹ in the form of a broad parallel beam. Using photon regeneration means that all primary photons that interact within the chamber geometry are regenerated at the point of interaction and all scattered photons are discarded, including all bremsstrahlung and fluorescence photons.^{4,5} This is equivalent to removing the effect of attenuation and scatter on the calculated response, and thus calculations of D_{air} are actually calculations of $D_{air}K_{wall}$. Photon regeneration is required for true charged particle equilibrium (CPE), which is assumed in the air kerma formalism. We will use the notation D_{air}^{Fano} such that

$$D_{air}^{Fano} = D_{air}K_{wall} \quad (5)$$

to distinguish from calculations of D_{air} without photon regeneration. The transport parameters in these calculations and cross sections are the same as those used previously.¹⁵ However, the choice of cross sections is unimportant since the analysis that follows depends upon the ratios of responses to

theory which, for graphite chambers, has been shown to be independent of the cross sections if a completely consistent set of cross-section data is used.^{3,5} We have confirmed that the same holds true for high-Z chambers within the statistical precision considered here.

Under the simulation conditions described above, the K_h , K_{an} , and K_{comp} corrections are unity by definition. Furthermore, the correction for additional nonideal conditions, K , reduces to a fluence correction, denoted here as K_{fl} , to correct for a potential perturbation of the wall’s charged particle fluence in the cavity gas. The K_{fl} correction replaces the K_{SA} correction^{5,6} discussed above because we are only dealing with ^{60}Co beams and not low-energy beams where other aspects of the theory break down. In particular, we assume that the fraction of response due to photon interactions in the cavity is negligible, which cannot be assumed for low-energy photons,^{5,22,23} and that the departure from SA conditions is primarily due to the perturbation of the charged particle fluence by the presence of the cavity. Thus, Eq. (1) reduces to

$$K_{air} = \frac{D_{air}}{(1 - \bar{g}_{air})} \left(\frac{\bar{L}_{\Delta}}{\rho} \right)_{air}^{wall} \left(\frac{\bar{\mu}_{en}}{\rho} \right)_{wall} K_{wall} K_{fl}. \quad (6)$$

Expressing the collision air kerma as $(K_c)_{air} = K_{air}(1 - \bar{g}_{air})$ and solving for $K_{fl}(\bar{L}_{\Delta}/\rho)_{air}^{wall}$ gives

$$K_{fl} \left(\frac{\bar{L}_{\Delta}}{\rho} \right)_{air}^{wall} = \frac{(K_c)_{air}}{D_{air}K_{wall}} \left(\frac{\bar{\mu}_{en}}{\rho} \right)_{air}^{wall} = \frac{(K_c)_{wall}}{D_{air}^{Fano}}, \quad (7)$$

which provides us with a way to indirectly calculate the product $K_{fl}(\bar{L}_{\Delta}/\rho)_{air}^{wall}$. Values of $(K_c)_{wall}$ are calculated using the g user code^{15,24} for each wall material in order to extract values of $K_{fl}(\bar{L}_{\Delta}/\rho)_{air}^{wall}$ from calculations of D_{air}^{Fano} . If the cavity is filled with a low-density wall material that has the same dosimetric properties as the wall, then from the Fano theorem^{10,25} the collision kerma in the wall, $(K_c)_{wall}$, is equal to the K_{wall} -corrected dose to the low-density wall material, denoted as $D_{wall, gas}^{Fano} \equiv D_{wall, gas}K_{wall}^{wall, gas}$, where $K_{wall}^{wall, gas}$ represents the correction for attenuation and scatter by the wall for a chamber filled with wall gas (to distinguish it from K_{wall}). In our case, the wall gas has the same density as air (1.205 kg/m³) but the ICRU density effect corrections for the stopping-power data sets are the same as the wall material with bulk density, as discussed in Ref. 26. Equation (7) may then be written as

$$K_{fl} \left(\frac{\bar{L}_{\Delta}}{\rho} \right)_{air}^{wall} = \frac{D_{wall, gas}^{Fano}}{D_{air}^{Fano}}. \quad (8)$$

Comparing calculations of $K_{fl}(\bar{L}_{\Delta}/\rho)_{air}^{wall}$ from Eqs. (7) and (8) is equivalent to performing the Fano cavity test for a range of wall materials and cavity dimensions [i.e., comparing $D_{wall, gas}^{Fano}$ to $(K_c)_{wall}$], which serves as a useful check of the transport mechanics of the code in addition to Fano tests performed previously. Detailed discussions of this test with EGSnrc can be found in Refs. 15, 20, 24, and 26.

TABLE I. Values of the mean chord length and Δ at each cavity height for the plane-parallel chamber (1.2 cm radius) used in this study. The mean chord length L was estimated as $4V/S$, while values of Δ were taken as the kinetic energy of an electron with a CSDA range in dry air= L . Also listed are the Spencer-Attix wall-to-air stopping-power ratios in a ^{60}Co beam for graphite, aluminum, copper, and lead calculated in a small phantom of material using SPRRZnrc with photon regeneration.

Cavity height (cm)	$L=4V/S$ (cm)	Δ (keV)	$\left(\frac{\bar{L}_\Delta}{\rho}\right)_{\text{air}}^{\text{wall}}$			
			Graphite	Al	Cu	Pb
0.05	0.096	5.7	1.002 60(8)	0.854 76(3)	0.703 7(1)	0.4817(2)
0.075	0.141	7.1	1.002 32(8)	0.857 41(2)	0.709 1(1)	0.4915(2)
0.1	0.185	8.3	1.002 17(8)	0.859 08(2)	0.712 68(7)	0.4975(2)
0.15	0.267	10.3	1.001 80(8)	0.861 38(2)	0.717 24(5)	0.5056(2)
0.2	0.343	12.0	1.001 51(8)	0.862 89(2)	0.720 24(5)	0.5107(2)
0.3	0.480	14.5	1.001 23(8)	0.864 57(2)	0.723 64(4)	0.5166(2)
0.4	0.600	16.6	1.001 12(8)	0.865 81(2)	0.726 04(4)	0.5205(2)
0.5	0.706	18.2	1.000 99(8)	0.866 59(2)	0.717 47(4)	0.5227(2)
0.6	0.800	19.6	1.000 98(8)	0.867 21(2)	0.728 69(4)	0.5249(2)
0.8	0.960	21.8	1.000 73(8)	0.868 00(2)	0.730 40(4)	0.5276(2)
1.0	1.091	23.4	1.000 66(8)	0.868 59(2)	0.731 48(3)	0.5293(2)
1.2	1.200	24.8	1.000 67(8)	0.869 01(2)	0.732 32(3)	0.5306(2)

II.B. Calculation of Spencer-Attix stopping-power ratios

The accuracy of the SA cavity theory as applied in Eq. (1) can be revealed through values of K_{fl} extracted from the calculations of $K_{fl}(\bar{L}_\Delta/\rho)_{\text{air}}^{\text{wall}}$ discussed above as a function of cavity height and the corresponding SA wall-to-air stopping-power ratios. Values of K_{fl} that are unity within statistical uncertainties are an indication that the underlying assumptions of the theory are applicable.

The SA wall-to-air restricted mass stopping-power ratios in ^{60}Co beams are calculated with the SPRRZnrc user code¹⁶ following the approach described by Borg *et al.*⁵ We are interested in stopping powers for an unattenuated, unscattered photon beam as the theory requires. Therefore, as for the CAVRZnrc calculations, these calculations were also performed with the photon regeneration option selected. The stopping-power ratio was scored in the central region of a uniform cylinder of wall material surrounded with enough material to provide full buildup. In principle, the results are independent of geometry.^{5,16} As in Sec. I A, the values of Δ for these calculations, which determine which set of restricted stopping powers is used in the simulations, were set to the kinetic energy of an electron with a CSDA range in air equal to L , given by $4V/S$. Since L depends on cavity size, separate PEGS4 data sets of restricted stopping powers were created for each corresponding value of Δ , where the threshold energy for the production of charged particles (AE) was set equal to $\Delta+511$ keV. This is unlike the calculation of chamber response where AE was set to 1 keV regardless of cavity size and which was previously shown to ensure accuracy of the results.¹⁵ Table I lists the values of L and Δ for each cavity height used with the idealized pp chamber along with the wall-to-air stopping-power ratios for graphite, aluminum, copper, and lead wall materials.

The calculations of SA wall-to-air stopping-power ratios were repeated for values of Δ from 1 to 60 keV in 1 keV intervals. A functional form for $(\bar{L}_\Delta/\rho)_{\text{air}}^{\text{wall}}$, given as

$$\left(\frac{\bar{L}_\Delta}{\rho}\right)_{\text{air}}^{\text{wall}} = a + b \ln(\Delta) + \frac{c}{\sqrt{\Delta}} + \frac{d}{\Delta^2}, \quad (9)$$

was then fitted to these calculations using the method of least squares, where a , b , c , and d represent the best fit coefficients (see Table II). Equation (9) reflects the monotonic trend of the stopping-power ratios as a function of Δ . In all cases, the fit was within 0.1% of the calculated values and within 0.03% for the graphite chamber.

II.C. Calculation of fluence correction factors (K_{fl})

Values of K_{fl} were obtained by dividing the calculated value of $K_{fl}(\bar{L}_\Delta/\rho)_{\text{air}}^{\text{wall}}$ [Eq. (7) or Eq. (8)] at each cavity height by the corresponding value of $(\bar{L}_\Delta/\rho)_{\text{air}}^{\text{wall}}$ listed in Table I (i.e., assuming the $L=4V/S$ prescription is correct). For these calculations, the average of $K_{fl}(\bar{L}_\Delta/\rho)_{\text{air}}^{\text{wall}}$ calculated

TABLE II. Values of fit coefficients for the least-squares fit of Eq. (9) to values of the SA stopping-power ratio as a function of Δ (1 keV \leq Δ \leq 60 keV) for a ^{60}Co beam.

Material	a	b	c	d
Beryllium	0.9176(4)	-0.001 68(7)	0.0140(6)	0.0009(3)
Graphite	1.0023(4)	-0.000 77(8)	0.0040(7)	0.0008(3)
Aluminum	0.8674(1)	0.003 22(2)	-0.0433(2)	-0.0036(1)
Copper	0.7317(2)	0.005 83(5)	-0.0897(4)	-0.0156(3)
Silver	0.6535(4)	0.006 97(9)	-0.1176(8)	-0.0310(4)
Tin	0.6294(6)	0.007 4(1)	-0.115(1)	-0.033(5)
Lead	0.529(1)	0.009 8(2)	-0.144(2)	-0.100(1)

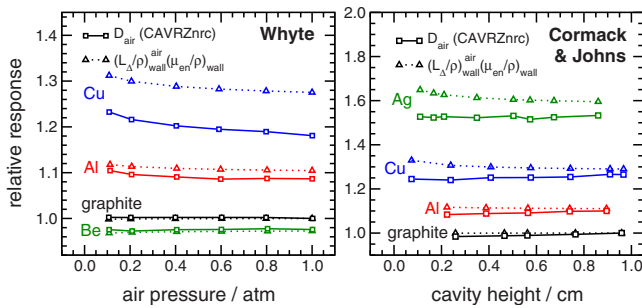


FIG. 1. EGSnrc-calculated values of response as a function of cavity air pressure for the Whyte chamber (Ref. 14) (relative to graphite chamber, 1 atm) and as a function of cavity height for the Cormack and Johns chamber (Ref. 13) (relative to graphite chamber, 0.96 cm cavity height). Also shown is the product of $(\bar{L}_\Delta/\rho)_{\text{wall}}^{\text{air}}$ and $(\bar{\mu}_{\text{en}}/\rho)_{\text{wall}}$ for each wall material, calculated as discussed in Secs. II B and II A.

from Eqs. (7) and (8) was used since, as we will show, the two methods give nearly the same numeric result and should be equivalent. Furthermore, using the average value of $K_{fl}(\bar{L}_\Delta/\rho)_{\text{air}}^{\text{wall}}$ reduces the statistical uncertainty on K_{fl} .

Values of K_{fl} were also calculated for several of the graphite-walled ion chambers used as ^{60}Co air kerma standards at national metrology institutes (NMIs). The graphite densities and dimensions of the various chambers were obtained from the references listed in the BIPM report by Allisy-Roberts *et al.*²⁷ but were modeled without insulating materials as the theory requires. As with all calculations with graphite in this investigation, the graphite stopping powers for these calculations correspond to those with an ICRU-recommended²⁸ mean ionization energy (I value) of 78 eV. While there is a real issue about what the proper I value is for graphite, using a different I value should have a negligible effect if the same I value is used for all calculations of K_{fl} for a given wall material. The effect of the graphite density and I value on calculations of K_{fl} is explored by calculating K_{fl} as a function of both. The effect of the incident spectrum and transport parameters on K_{fl} is also investigated.

III. RESULTS AND DISCUSSION

III.A. Limitations of Spencer-Attix cavity theory

The accuracy of the SA cavity theory was tested by comparing the calculated response of chambers used by Cormack and Johns in 1954 (Ref. 13) and Whyte in 1957 (Ref. 14) to the values calculated with Eq. (4). The results are shown in Fig. 1 for wall materials ranging from beryllium to silver. Relative to the response of the graphite chamber at atmospheric pressure (Whyte chamber) or with a 0.95 cm cavity height (Cormack and Johns chamber), the response predicted by the SA cavity theory without correction factors [Eq. (4)] differs in magnitude from CAVRZnrc calculations, and hence from measurements, by as much as 8.5%. Equation (4) also fails to predict the response with changes in cavity height or air pressure in some cases. However, the predicted variation in response of the graphite chamber, to the extent

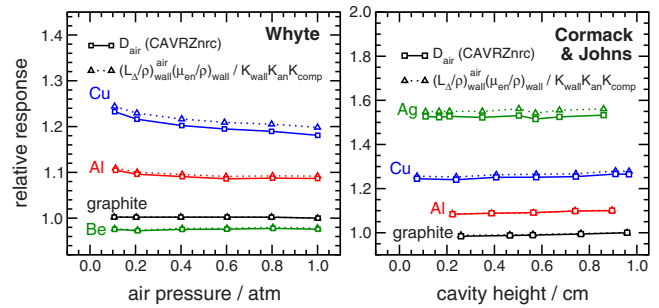


FIG. 2. As in Fig. 1 with values of $(\bar{L}_\Delta/\rho)_{\text{wall}}^{\text{air}}(\bar{\mu}_{\text{en}}/\rho)_{\text{wall}}$ corrected by calculated values of $K_{\text{wall}}K_{\text{an}}K_{\text{comp}}$.

that there is variation, is within 0.3% and 1.5% for the Whyte¹⁴ and Cormack and Johns¹³ chambers, respectively.

Strictly speaking, the predictions of the SA cavity theory only apply to the response of chambers under ideal conditions. Thus, values of D_{air} calculated directly by CAVRZnrc should be corrected by K_{wall} , K_{an} , and K_{comp} for more meaningful comparisons. Alternatively, $(\bar{L}_\Delta/\rho)_{\text{wall}}^{\text{air}}(\bar{\mu}_{\text{en}}/\rho)_{\text{wall}}$ could be divided by these correction factors. Using the approach of previous Monte Carlo studies,^{3,4} K_{wall} , K_{an} , and K_{comp} were calculated for each chamber configuration. Since dry air is used in these simulations, K_h is unity, and so is K since there are no other nonideal conditions to correct for in the simulation of these experiments. Figure 2 compares the fully corrected SA predicted values of D_{air} as in Fig. 1. Although some discrepancies larger than 1% still remain for high- Z chambers, the overall agreement is significantly improved. For the Whyte chamber, the improvement is mostly due to the effect of the K_{wall} and K_{an} corrections on the relative magnitude of the responses rather than the response as a function of pressure. For the Cormack and Johns chamber, the use of correction factors improved agreement both in terms of the relative magnitude of the predicted response and the variation with cavity height.

The effect of each individual correction for the Whyte chamber with copper walls is shown in Fig. 3. In this example, the effect on response of the K_{wall} correction relative to the K_{wall} correction for graphite is shown to be much larger than the relative effect of the K_{an} and K_{comp} corrections. A 1.5%–2.0% discrepancy remains between the calculated response and the fully corrected SA prediction in this case, and similar discrepancies are observed with the Cormack and Johns chamber. These remaining discrepancies are not related to uncertainties in cross-section data since the cross sections used were common to both sets of calculations in this comparison. Rather, this discrepancy is attributed to the perturbation of the charged particle fluence by the cavity, and an additional fluence correction (K_{fl}) is therefore required.

III.B. Perturbation of charged particle fluence by the cavity

The need for a fluence correction can be seen by examining the effect of a cavity on the charged particle fluence in

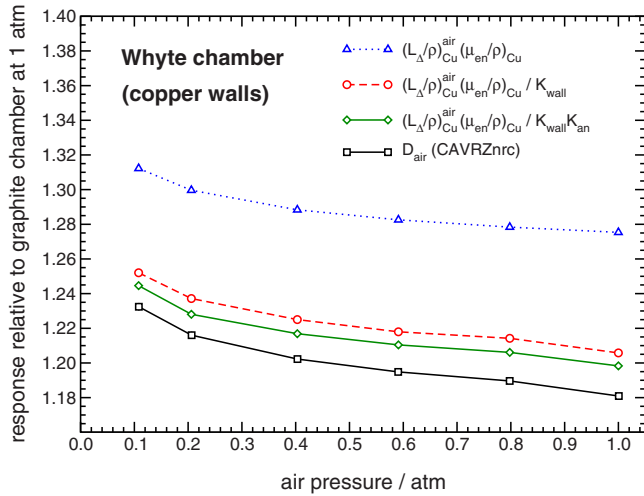


FIG. 3. As in Figs. 1 and 2 for the Whyte chamber with copper walls. The relative effect of each correction factor on the comparison is also shown by dividing the values of $(\bar{L}_\Delta/\rho)_{Cu}^{air}(\mu_{en}/\rho)_{Cu}$ by one correction at a time. The effect of the K_{comp} correction is small ($<0.1\%$) relative to the effect of K_{wall} and K_{an} and is therefore not included in this plot.

the wall medium. Figure 4 shows the EGSnrc-calculated spectrum of charged particles in the cavity region of the idealized plane-parallel ion chamber described in Sec. II A for two cavity sizes and wall materials. Photon regeneration was used in these calculations since we are interested in the case where the effects of attenuation and scatter have been removed. Otherwise, this calculation is similar to one performed in a previous investigation.²⁹

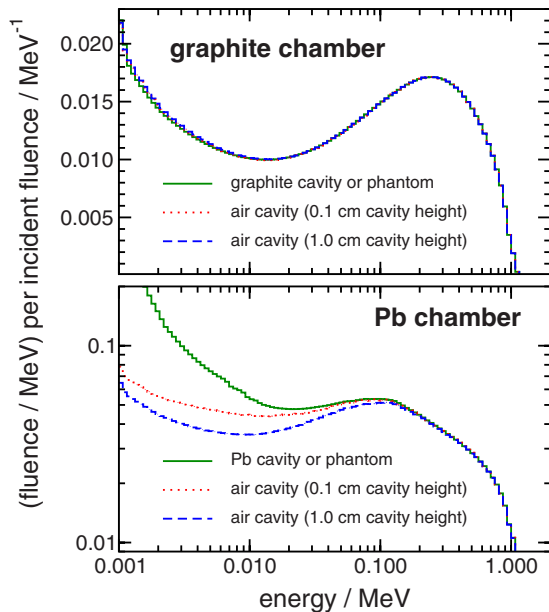


FIG. 4. Fluence of charged particles in the cavity region of an idealized plane-parallel ion chamber in a ^{60}Co beam (described in Sec. II A). The effects of attenuation and scatter have been removed by using photon regeneration. Results are shown for 0.1 and 1.0 cm cavity heights and for wall materials of graphite and lead. The solid lines are for low-density wall material in the cavity and are identical to spectra calculated in a wall phantom as expected from the Fano theorem.

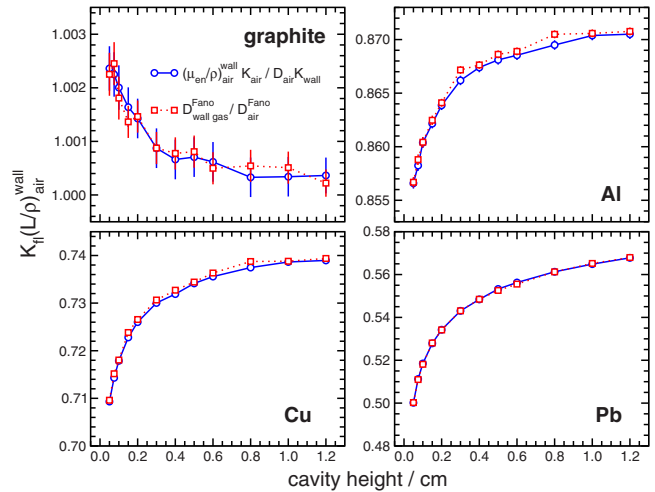


FIG. 5. Values of $K_{fl}(\bar{L}_\Delta/\rho)_{air}^{wall}$ calculated as discussed in Sec. II A for graphite, aluminum, copper, and lead wall materials.

Fluence spectra were calculated for cavities filled with either air or wall material. As shown, the air cavity appears to have only a small effect on the fluence in the graphite wall regardless of cavity size. For the extreme case of a lead chamber, the air cavity reduces the charged particle fluence significantly at low energies (i.e., <0.1 MeV). Given the results shown in Fig. 4, one could argue that fluence corrections should be included in the air kerma formalism regardless of whether or not they could be made unity via an appropriate selection of Δ in the SA stopping-power ratio. However, the fluence perturbations occur primarily at low energies, and may therefore not affect the evaluation of the SA stopping-power ratio since it only considers the fluence above Δ (recall that the track-end term does not include charged particles *created* below Δ , only those that “slow down” to that energy). For example, the fluence perturbation for the graphite chamber is only visible below about 10 keV and about 50–60 keV for the lead chamber (1.0 cm cavity height). Calculations for aluminum and copper chambers reveal that fluence perturbations occur primarily below 30 and 40 keV, respectively. Thus the need for fluence corrections will depend on whether or not there exists a value of Δ that can exclude *a priori*.

III.C. Calculations of $K_{fl}(\bar{L}_\Delta/\rho)_{air}^{wall}$

Values of $K_{fl}(\bar{L}_\Delta/\rho)_{air}^{wall}$ obtained from CAVRZnrc calculations as a function of cavity height using the two methods described in Sec. II A are shown in Fig. 5 for graphite, aluminum, copper, and lead wall materials. The differences between the results of the two methods should be negligible due to the Fano theorem. The agreement between the two sets of calculations serves to further validate the transport mechanics of the EGSnrc code. Of particular significance is the agreement observed with copper and lead, where the root mean squared deviations of the ratio of the two results from unity are 0.09% and 0.06%, respectively. Statistical uncer-

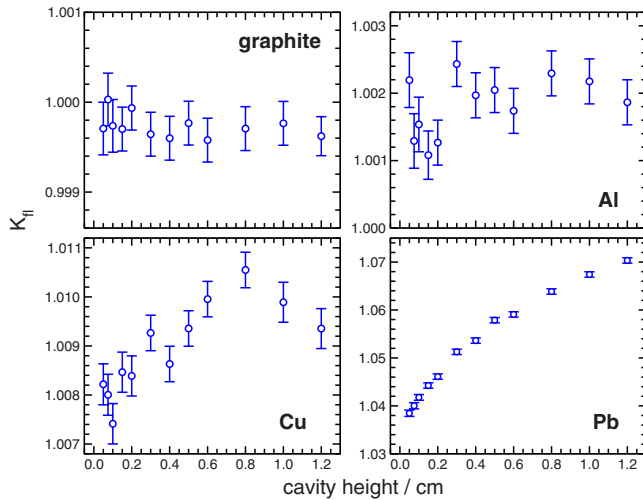


FIG. 6. Values of K_{fl} as a function of cavity height calculated on the assumption that the standard prescription for Δ is correct and using the average value of $K_{fl}(\bar{L}_\Delta/\rho)_{air}^{wall}$ from Fig. 5 divided by the corresponding value of $(\bar{L}_\Delta/\rho)_{air}^{wall}$ from Table I.

tainties on the calculated values are 0.1% or less. Similar agreement was also obtained for wall materials of beryllium and tin.

III.D. Fluence correction factors (K_{fl}) for the air kerma formalism

In this section we investigate the size of K_{fl} on the assumption that the standard $L=4V/S$ method for assigning Δ is correct. Figure 6 shows values of K_{fl} as a function of cavity height for the same four wall materials as in Fig. 5. The approach to calculating K_{fl} is described in Sec. II C. For the graphite chamber, K_{fl} values are very close to unity, although on average they are below unity by 0.03%. Values of K_{fl} close to unity are expected for graphite chambers since graphite is nearly air equivalent at ^{60}Co energies. By the Fano theorem, the perturbation of the charged particle fluence by the cavity is negligible regardless of cavity size and air density.

As the atomic number (Z) of the wall increases relative to the effective Z of the air, values of K_{fl} increase above unity. As with the graphite chamber, there does not appear to be a trend in K_{fl} with cavity height for the aluminum chamber, but the corrections are larger [average value of 1.0018(1)]. A slight trend is observed for the copper chamber, and values of K_{fl} are as high as 1% in some cases. For the lead chamber, the value of K_{fl} is strongly dependent on the cavity size, ranging from 1.0385(6) at a cavity height of 0.05 cm to 1.0703(6) at a cavity height of 1.2 cm. This is qualitatively consistent with Fig. 4 where the electron fluence spectrum was shown to differ more for the large cavity. Similar results were obtained for the chamber with tin walls, only with less variation. The K_{fl} corrections for the chamber modeled with beryllium walls, the Z of which is less than the effective Z of air, are less than unity [average value of 0.9991(1)] and also slightly less on average than the K_{fl} values for the graphite

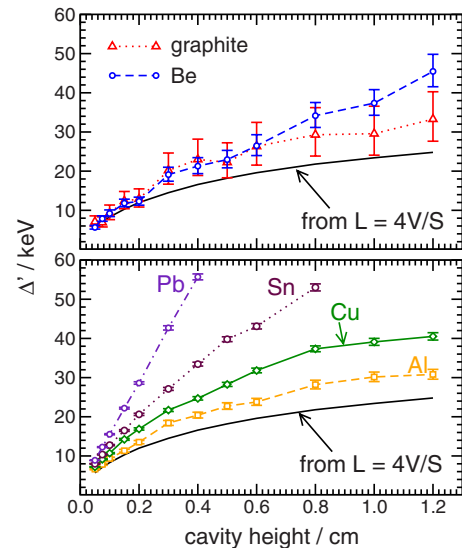


FIG. 7. Values of Δ' for $(\bar{L}_{\Delta'}/\rho)_{air}^{wall}$ required to avoid a nonunity value of K_{fl} as a function of cavity height. Also shown are the values of Δ' equal to the kinetic energy of an electron with a CSDA range in air given by $L=4V/S$.

chamber. In general, based on these results, K_{fl} diverges from unity as the difference between the (effective) Z of air and wall material increases.

III.E. Extraction of Δ from values of $K_{fl}(\bar{L}_\Delta/\rho)_{air}^{wall}$

The calculation of K_{fl} corrections discussed in Sec. III D assumes *a priori* that the choice of Δ in the calculation of the SA wall-to-air stopping-power ratio is appropriate. Janssens³⁰ proposed a different definition of Δ which takes into account the fact that many low-energy electrons do not escape because they backscatter from the walls even if they have the energy to cross the cavity. Although this proposed change may be appropriate, it makes Δ more difficult to determine.

Insight into the value of Δ that should be used can be obtained by analyzing the calculated values of $K_{fl}(\bar{L}_\Delta/\rho)_{air}^{wall}$ assuming $K_{fl} \equiv 1.000$; i.e., we equate values of $K_{fl}(\bar{L}_\Delta/\rho)_{air}^{wall}$ to $(\bar{L}_{\Delta'}/\rho)_{air}^{wall}$ to determine the corresponding value of Δ' . If the extracted values of Δ' are independent of wall material but not necessarily the same as the value of Δ corresponding to L , then this would indicate that the standard prescription for choosing Δ is wrong, and no K_{fl} correction would be needed in the air kerma formalism. Using the average value of $K_{fl}(\bar{L}_\Delta/\rho)_{air}^{wall}$ at each cavity height in Fig. 5, Eq. (9) along with the fit coefficients in Table II were used to systematically find the corresponding values of Δ' as a function of cavity height for each wall material. The results are shown in Fig. 7 with the data for graphite and beryllium wall materials separated from the data for the other materials for clarity of presentation. Uncertainties on Δ' were estimated from the standard deviation (σ) on the $K_{fl}(\bar{L}_\Delta/\rho)_{air}^{wall}$ values (in Fig. 5) from which it was derived, where the upper limit on Δ' is taken from $K_{fl}(\bar{L}_\Delta/\rho)_{air}^{wall} + \sigma$ and the lower limit from

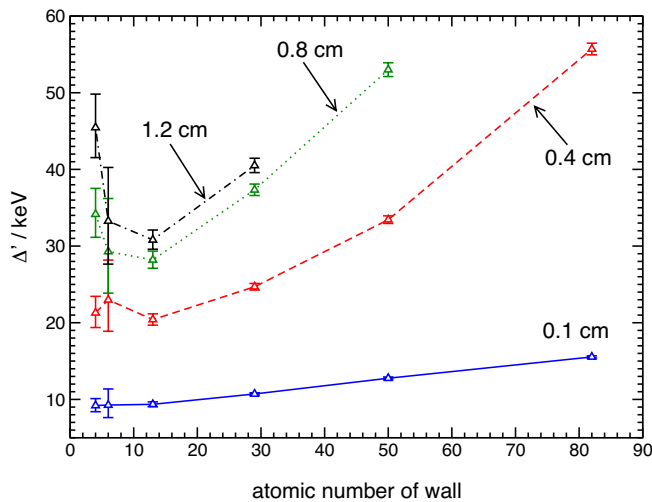


FIG. 8. Values of Δ' for $(\bar{L}_\Delta/\rho)_{air}^{wall}$ as a function of the atomic number of the chamber wall material for cavity heights of 0.1, 0.4, 0.8, and 1.2 cm. Values were extracted as discussed in Secs. II B and III E.

$K_{fl}(\bar{L}_\Delta/\rho)_{air}^{wall} - \sigma$. As a result, the uncertainties on Δ' for the graphite chamber are larger since the SA graphite-to-air stopping-power ratio is relatively insensitive to this parameter. Also shown in Fig. 7 for comparison is the variation in Δ expected from the $L=4V/S$ prescription (see Sec. I A). With the exception of the graphite and beryllium chambers at cavity heights ≤ 0.2 cm, Δ' is larger than the kinetic energy of an electron with a CSDA range in air equal to L . The difference between the extracted and expected values increases with cavity height. For the tin and lead chambers, values of Δ' were not obtained above cavity heights of 0.8 and 0.4 cm, respectively, since $(\bar{L}_\Delta/\rho)_{air}^{wall}$ data were not calculated for $\Delta > 60$ keV. However, it was confirmed through calculations of $(\bar{L}_\Delta/\rho)_{air}^{wall}$ with larger Δ values that corresponding values of Δ' can be obtained for all the cavity heights for these two chambers.

If one accepts the definition for Δ (or Δ') proposed by Janssens,³⁰ then to account for charged particles that cross but backscatter into the cavity the value needed to avoid K_{fl} corrections should be larger than the kinetic energy of an electron needed to travel a distance L in air. Based on this reasoning, it should be expected that Δ' increases as the atomic number of the chamber wall increases since the backscatter coefficient for electrons also increases with Z for a given energy.³¹ For the chamber investigated here, Fig. 8 shows that Δ' does in fact increase as Z of the wall increases for a cavity height of 0.1 cm, although the uncertainty on the value for the graphite wall ($Z=6$) is relatively large. The same cannot be said, however, for the trend in Δ' with atomic number at larger cavity heights. At cavity heights of 0.8 and 1.2 cm, Δ' clearly decreases from $Z=4$ (beryllium) to $Z=13$ (aluminum) and then begins to increase again, contrary to the expectation mentioned above. In any case, the value of Δ' needed to avoid K_{fl} corrections clearly depends on Z in addition to the cavity dimensions.

III.F. On calculating K_{fl} directly

The calculation of the K_{fl} corrections shown in Fig. 6 was based on assumptions about the value of Δ for a given cavity size. Ideally, however, one should be able to calculate K_{fl} independently of these assumptions, perhaps by using the methods to calculate P_{repl} for chambers in phantom. In a recent paper,²⁹ methods were presented for directly calculating the replacement correction factor P_{repl} . This corresponds to the K_{fl} correction for in-air calculations. However, in endeavoring to use these methods here for high- Z materials it became clear that these methods are not applicable. This is discussed further elsewhere.³²

III.G. K_{fl} values for graphite-walled chambers

The EGSnrc-calculated values of K_{fl} for the graphite-walled ion chambers used at NMI laboratories are shown in Table III. All values are calculated to a statistical precision of 1 part in 10^4 . Values ranged between 0.9996 and 0.9999 and there does not appear to be a trend with cavity size or chamber type. Also listed in Table III are the SA graphite-to-air stopping-power ratios $(\bar{L}_\Delta/\rho)_{air}^{wall}$ used to calculate K_{fl} and the associated values of Δ . Values of $(\bar{L}_\Delta/\rho)_{air}^{wall}$ are calculated on the assumption that Δ is properly determined using the $L=4V/S$ rule.

III.H. Uncertainties on K_{fl} for graphite chambers

The uncertainties on K_{fl} quoted in Table III for the graphite chambers used at the NMIs represent one standard deviation statistical uncertainties for a given set of transport parameters and cross-section data sets. The following sections discuss the sensitivity of calculated K_{fl} values for graphite chambers to the density and I value of graphite, incident spectrum, photon cross sections, and electron transport parameters.

III.H.1. Effect of density and mean ionization energy on K_{fl} calculations

In previous investigations, it was shown that, combined, the density effect and I value of graphite can have a large effect (i.e., 1.5% or more) on the calculated response of graphite chambers⁶ and on calculations of the SA graphite-to-air stopping-power ratio.³ Although these large effects likely cancel when computing values of K_{fl} , the effects of both the density and I value on K_{fl} were examined at the level of statistical uncertainty considered here.

Figure 9 shows calculations of K_{fl} for the plane-parallel graphite chamber as a function of the density of the graphite wall. Calculations were repeated for cavity heights of 0.15 and 0.6 cm and I values of 78 and 87 eV. For each calculation, the density effect for graphite was calculated using the ESTAR program from NIST.³³ Values of the calculated response varied by nearly 2% from the lowest value ($I=78$ eV, $\rho=1.7$ g/cm³) to the highest value ($I=87$ eV, $\rho=2.26$ g/cm³). Despite this variation, calculations of K_{fl} are independent of both the density and I value. The average value of K_{fl} is 0.999 89(4) for the 0.15 cm cav-

TABLE III. EGSrc-calculated values of K_{fl} for the graphite-walled chambers used as ^{60}Co air kerma standards at various national metrology institutes. Details about the various chambers may be found in a report by Allisy-Roberts *et al.* (Ref. 27) and references therein. The uncertainties on $(\bar{L}_\Delta/\rho)_{\text{air}}^{\text{wall}}$ and K_{fl} represent the statistical uncertainties for one standard deviation.

NMI	Chamber type	ρ_{graphite} (g/cm ³)	$L=4V/S$ (cm)	Δ (keV)	$(\bar{L}_\Delta/\rho)_{\text{air}}^{\text{wall}} \pm 0.00002$	$K_{fl} \pm 0.0001$
BEV	Cylindrical	1.72	0.65	17.3	1.001 05	0.9999
		1.80	0.65	17.3	1.001 05	0.9999
NMi	Spherical	1.8045	1.40	27.1	1.000 56	0.9999
NIST	Spherical, 30cc	1.74	2.57	38.6	1.000 18	0.9999
	Spherical, 50cc	1.74	3.07	42.8	1.000 02	0.9997
ARPANSA	BIPM-type	1.73	0.41	13.3	1.001 38	0.9997
VNIIM	Cylindrical, 1cc	1.634	0.66	17.6	1.001 10	0.9997
	Cylindrical, 30cc	1.634	2.26	35.8	1.000 24	0.9999
NRC	Cylindrical	1.66	0.76	19.0	1.001 01	0.9998
PTB	Cylindrical HRK1	1.775	0.45	14.0	1.001 36	0.9998
	Cylindrical HRK2	1.775	0.67	17.9	1.001 07	0.9996
	Spherical HRK3	1.775	0.40	13.0	1.001 40	0.9997
SMU	Cylindrical	1.71	0.64	17.2	1.001 04	0.9999
ZMDM	Cylindrical	1.75	0.64	17.2	1.001 04	0.9999
NMIJ	Cylindrical 6cc	1.85	1.25	25.3	1.000 68	0.9997
	Cylindrical, 63cc	1.85	2.76	40.3	1.000 11	0.9997
NCM	Cylindrical	1.75	0.64	17.2	1.001 04	0.9999
LNMRI	Cylindrical	1.71	0.64	17.2	1.001 04	0.9999
LNE-LNHB	Cylindrospherical	1.81	1.60	29.3	1.000 47	0.9999
ENE	Cylindrical	1.75	0.64	17.2	1.001 04	0.9999
MKEH	Cylindrical	1.75	0.65	17.3	1.001 05	0.9998
BIPM	Parallel plate	1.84	0.41	13.2	1.001 45	0.9996

ity height and 0.999 73(3) for the 0.6 cm cavity height. In each case, the root mean squared deviation is $\approx 0.008\%$, which is comparable to the statistical uncertainty on each value. Since only 4 of the 12 values deviate from the average by more than one standard deviation, there is no indication of any statistically significant variation. As such, the systematic uncertainty associated with the restricted stopping powers used is estimated to be 1 part in 10^4 .

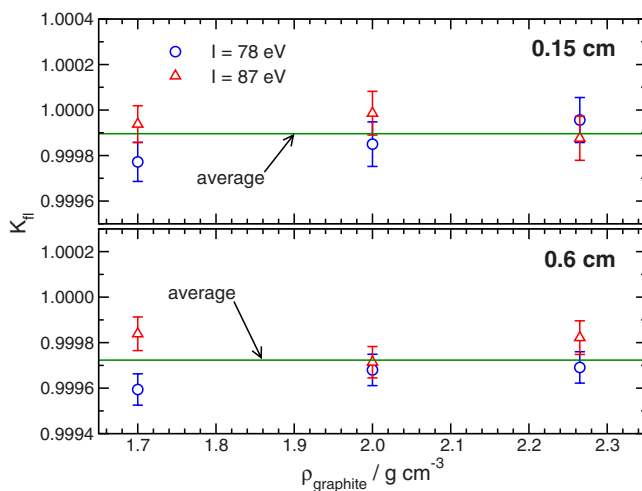


FIG. 9. Calculations of K_{fl} for plane-parallel graphite chambers of two cavity sizes as a function of the graphite density and l values used to calculate the graphite stopping powers.

III.H.2. Effect of the incident spectrum and photon cross sections

The effect of the incident spectrum and photon cross sections on calculated values of K_{fl} was investigated using five different photon sources at ^{60}Co energies. These include a 1.25 MeV monoenergetic photon source, a spectrum representing a bare ^{60}Co source with two equiprobable photon lines at 1.175 and 1.334 MeV, a ^{60}Co spectrum published in 1988,³⁴ and two ^{60}Co spectra calculated by Mora *et al.* for 10×10 and 30×30 field sizes.²¹ The 10×10 spectrum is that used throughout the rest of this investigation.

Figure 10 shows that the variation of calculated K_{fl} values for the realistic spectra is approximately 0.01% (RMSD=0.004%), which is comparable to the statistical uncertainties on those calculations. A slightly larger, 0.02%–0.03%, increase in K_{fl} is observed as one changes from a realistic spectrum to a monoenergetic or bare ^{60}Co source. All of these imply that calculations of K_{fl} are insensitive to the details of the incident realistic spectrum, which contributes no more than 0.01% to the overall uncertainty on K_{fl} .

The effect of the photon cross sections was also investigated by comparing values of K_{fl} calculated with cross sections compiled by Storm and Israel³⁵ with those calculated using the XCOM cross sections from NIST.^{36,37} Values of K_{fl} for 0.6 cm cavity height were within 0.003% in this comparison. The differences between these cross sections for graphite are less than 0.003% at ^{60}Co energies (1.25 MeV)

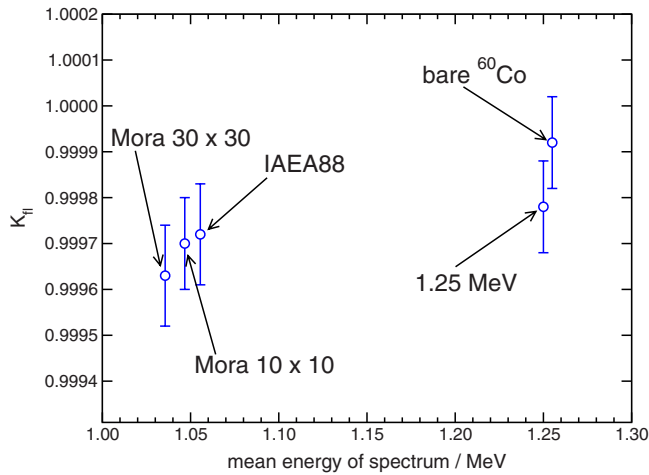


FIG. 10. Values of K_{fl} calculated for various incident photon spectra at ^{60}Co energies.

but increases to over 1% as at lower energies. Increasing the photon cross sections more dramatically by 1% and 5% also had about a 0.01% effect on the value of K_{fl} .

III.H.3. Effect of electron transport parameters

In the EGSnrc Monte Carlo code, an electron energy of 512 keV (1 keV kinetic energy) is considered the lower limit at which charged particles can be reliably tracked. Tracking charged particles below a kinetic energy of 1 keV is possible in EGSnrc,³¹ but the accuracy of the stopping powers below that energy, which are derived from the Beth-Block formalism, becomes questionable (or even higher energies than that for higher-Z materials). Generally, a cutoff energy (ECUT) of 521 keV is acceptable for graphite chambers for a statistical precision of about 0.1%,¹⁵ but calculations by Mainegra-Hing *et al.*¹⁹ showed that smaller cutoff energies are required for some plane-parallel graphite chambers for high-precision calculations. In this investigation, an ECUT of 512 keV was used for all ion chamber calculations but there may be a contribution to the overall uncertainty on K_{fl} at the level of precision considered here due to terminating charged particle histories at this energy. Using the parallel plate chamber with 0.05 and 0.6 cm cavity heights, values of K_{fl} were compared for cutoff energies of 512, 513, 516, and 521 keV (where $AE=ECUT$ in all cases). For the 0.6 cm cavity height, all calculated values of K_{fl} (with a statistical precision of 0.004%) are within 0.005% of values calculated

with $ECUT=512$ keV. Calculations are also within 0.005% for the chamber with a 0.05 cm cavity height (the smallest cavity size considered in this paper) when $ECUT=513$ keV, but differ by 0.05% and 0.1% for ECUT values of 516 and 521 keV, respectively. In any case, using a 1 keV kinetic energy cutoff should contribute no more than 1 part in 10^4 to the uncertainty in K_{fl} .

EGSnrc parameters related to charged particle transport were also investigated concerning the effect on calculated K_{fl} values. Excluding spin effects from the multiple scattering algorithm in EGSnrc changed calculated K_{fl} values by less than 0.005% (0.6 cm cavity height). Similar results were obtained for electron impact ionization on and off.

III.H.4. Summary of systematic uncertainties

Table IV summarizes the various contributions to the systematic uncertainty on calculated K_{fl} values for the graphite chambers discussed above. The overall uncertainty is approximately 0.02%. Although this is comparable to the average size of the correction, there were no cases where the calculated correction was unity or above. One can safely say that K_{fl} is within 0.04% of unity for all graphite-walled ion chambers studied, with an average value of 0.9998.

IV. CONCLUSIONS

In this investigation, EGSnrc calculations of chamber response were used to evaluate the accuracy of the Spencer-Attix cavity theory as it applies to the air kerma formalism. Using simulations of two classic experiments as an example, it was shown that the SA cavity theory generally fails to predict the response of ion chambers to ^{60}Co beams when no fluence correction factors are used. Following this, precise values of $K_{fl}(\bar{L}_{\Delta}/\rho)_{air}^{wall}$ were indirectly obtained from calculations of chamber response as a function of cavity size and wall material. Contrary to the assumptions of SA cavity theory, unit values of K_{fl} are not obtained in general when the low-energy cutoff Δ in the Spencer-Attix stopping-power ratio, $(\bar{L}_{\Delta}/\rho)_{air}^{wall}$, is set to the kinetic energy of an electron with a CSDA range in air equal to $4V/S$. However, when nearly air-equivalent walls such as graphite are used, K_{fl} values are within 0.04% of unity since Fano conditions are approximated. This applies to the graphite ion chambers used for ^{60}Co air kerma standards at national metrology institutes. For other wall materials, the size of the K_{fl} correction increases as the atomic number of the wall increases. As an alternative

TABLE IV. Summary of one standard deviation uncertainties on the calculation of K_{fl} for graphite chambers.

Component	Standard deviation uncertainty (%)	Comment
Stopping powers	0.01	Combines the effect of density and I value
Incident spectrum	0.01	Applies to realistic ^{60}Co spectra
Photon cross sections	0.01	Estimated from comparison of K_{fl} values calculated with two different photon cross sections
Transport parameters	0.01	
Overall	0.02	Including statistical uncertainties

to using K_{fl} corrections, one can select a low-energy cutoff Δ' in the SA stopping-power ratio such that K_{fl} corrections can be avoided. It is not obvious how to calculate Δ' from first principles but it can be obtained, as we have shown, using Monte Carlo methods. It was hoped that a simple relationship existed between Δ' and cavity size independent of the composition of the wall, but this is clearly not the case. Thus, given the complexity of calculating Δ' , it may be preferable to incorporate K_{fl} corrections in the air kerma formalism and always calculate the product of $K_{fl}(\bar{L}_\Delta/\rho)_{air}^{wall}$ rather than the individual factors.

ACKNOWLEDGMENTS

This research was enabled through the support of the Natural Sciences and Engineering Research Council of Canada (NSERC) through a Post Graduate Fellowship and a Discovery grant, the Canada Research Chairs (CRC) program, the Canada Foundation for Innovation (CFI), and the Ontario Innovation Trust (OIT). The authors wish to thank Ehsayed Ali for his helpful comments.

^{a)}Electronic mail: dlarussa@toh.on.ca

^{b)}Electronic mail: drogers@physics.carleton.ca;

URL: <http://physics.carleton.ca/clrp>

- ¹D. W. O. Rogers, in *Advances in Radiation Oncology Physics*, Medical Physics Monograph No. 19, edited by J. Purdy (AAPM, New York, 1992), pp. 181–223.
- ²A. F. Bielajew, "Ionization cavity theory: A formal derivation of perturbation factors for thick-walled ion chambers in photon beams," *Phys. Med. Biol.* **31**, 161–170 (1986).
- ³D. W. O. Rogers and I. Kawrakow, "Monte Carlo calculated correction factors for primary standards of air-kerma," *Med. Phys.* **30**, 521–543 (2003).
- ⁴D. T. Burns, "A new approach to the determination of air kerma using primary-standard cavity ionization chambers," *Phys. Med. Biol.* **51**, 929–942 (2006).
- ⁵J. Borg, I. Kawrakow, D. W. O. Rogers, and J. P. Seuntjens, "Monte Carlo study of correction factors for Spencer-Attix cavity theory at photon energies at or above 100 keV," *Med. Phys.* **27**, 1804–1813 (2000).
- ⁶L. A. Buckley, I. Kawrakow, and D. W. O. Rogers, "An EGSnrc investigation of cavity theory for ion chambers measuring air kerma," *Med. Phys.* **30**, 1211–1218 (2003).
- ⁷L. V. Spencer and F. H. Attix, "A theory of cavity ionization," *Radiat. Res.* **3**, 239–254 (1955).
- ⁸F. H. Attix, L. DeLa Vergne, and V. H. Ritz, "Cavity ionization as a function of wall material," *J. Res. Natl. Bur. Stand.* **60**, 235–243 (1958).
- ⁹T. E. Burlin, "An experimental examination of theories relating the absorption of γ -ray energy in a medium to the ionization produced in a cavity," *Phys. Med. Biol.* **6**, 33–53 (1961).
- ¹⁰F. H. Attix, *Introduction to Radiological Physics and Radiation Dosimetry* (Wiley, New York, 1986).
- ¹¹A. E. Nahum, "Water/air stopping-power ratios for megavoltage photon and electron beams," *Phys. Med. Biol.* **23**, 24–38 (1978).
- ¹²U. H. Nyström and A. E. Nahum, "A re-examination of the Spencer-Attix cavity integral," *Phys. Med. Biol.* **37**, 2143–2146 (1992).
- ¹³D. V. Cormack and H. E. Johns, "The measurement of high-energy radiation intensity," *Radiat. Res.* **1**, 133–157 (1954).
- ¹⁴G. N. Whyte, "Measurement of the Bragg-Gray stopping power correction," *Radiat. Res.* **6**, 371–379 (1957).
- ¹⁵D. J. La Russa and D. W. O. Rogers, "Accuracy of EGSnrc calculations of the response of various ion chambers to ^{60}Co beams," *Med. Phys.* **35**,

5629–5640 (2008).

- ¹⁶D. W. O. Rogers, I. Kawrakow, J. P. Seuntjens, and B. R. B. Walters, "NRC user codes for EGSnrc," National Research Council of Canada Technical Report No. PIRS-702, 2000, <http://www.irs.inms.nrc.ca/inms/irs/EGSnrc/EGSnrc.html>.
- ¹⁷I. Kawrakow, "Accurate condensed history Monte Carlo simulation of electron transport. I. EGSnrc, the new EGS4 version," *Med. Phys.* **27**, 485–498 (2000).
- ¹⁸I. Kawrakow and D. W. O. Rogers, "The EGSnrc code system: Monte Carlo simulation of electron and photon transport," National Research Council of Canada Technical Report No. PIRS-701, 2007, <http://www.irs.inms.nrc.ca/inms/irs/EGSnrc/EGSnrc.html>.
- ¹⁹E. Mainegra-Hing, I. Kawrakow, and D. W. O. Rogers, "Calculations for plane-parallel ion chambers in ^{60}Co beams using the EGSnrc Monte Carlo code," *Med. Phys.* **30**, 179–189 (2003).
- ²⁰I. Kawrakow, "Accurate condensed history Monte Carlo simulation of electron transport. II. Application to ion chamber response simulations," *Med. Phys.* **27**, 499–513 (2000).
- ²¹G. Mora, A. Maio, and D. W. O. Rogers, "Monte Carlo simulation of a typical ^{60}Co therapy source," *Med. Phys.* **26**, 2494–2502 (1999).
- ²²C.-M. Ma and A. E. Nahum, "Bragg-Gray theory and ion chamber dosimetry for photon beams," *Phys. Med. Biol.* **36**, 413–428 (1991).
- ²³D. J. La Russa and D. W. O. Rogers, "An EGSnrc investigation of the P_{TP} correction factor for ion chambers in kilovoltage x-rays," *Med. Phys.* **33**, 4590–4599 (2006).
- ²⁴J. P. Seuntjens, I. Kawrakow, J. Borg, F. Hobeila, and D. W. O. Rogers, in "Recent developments in accurate radiation dosimetry," *Proceedings of the International Workshop*, edited by J. P. Seuntjens and P. Mobit (Medical Physics, Madison, WI, 2002), pp. 69–84.
- ²⁵U. Fano, "Note on the Bragg-Gray cavity principle for measuring energy dissipation," *Radiat. Res.* **1**, 237–240 (1954).
- ²⁶D. W. O. Rogers, "Fifty years of Monte Carlo simulations for medical physics," *Phys. Med. Biol.* **51**, R287–R301 (2006).
- ²⁷P. J. Allisy-Roberts, D. T. Burns, and C. Kessler, "Summary of the BIPM.RI(I)-K1 comparison for air kerma in ^{60}Co gamma radiation," *Metrologia* **44**, 06006 (2007).
- ²⁸ICRU, "Stopping powers for electrons and positrons," ICRU Report No. 37 (ICRU, Washington, DC, 1984).
- ²⁹L. L. W. Wang and D. W. O. Rogers, "Calculation of the replacement correction factors for ion chambers in megavoltage beams by Monte Carlo simulation," *Med. Phys.* **35**, 1747–1755 (2008).
- ³⁰A. C. A. Janssens, "Modified energy-deposition model, for the computation of the stopping-power ratio for small cavity sizes," *Phys. Rev. A* **23**, 1164–1176 (1981).
- ³¹E. S. M. Ali and D. W. O. Rogers, "Benchmarking EGSnrc in the kilovoltage energy range against experimental measurements of charged particle backscatter coefficients," *Phys. Med. Biol.* **53**, 1527–1543 (2008).
- ³²L. L. W. Wang, D. J. La Russa, and D. W. O. Rogers, "Systematic uncertainties in the Monte Carlo calculation of ion chamber replacement correction factors," *Med. Phys.* **36**, 1785–1789 (2009).
- ³³M. J. Berger, "ESTAR, PSTAR and ASTAR: computer programs for calculating stopping-power and ranges for electrons, protons, and helium ions," NIST Report No. NISTIR-4999, 1992, available online at <http://physics.nist.gov/Star>.
- ³⁴D. W. O. Rogers, G. M. Ewart, A. F. Bielajew, and G. van Dyk, "Calculation of electron contamination in a ^{60}Co therapy beam," *Proceedings of the IAEA International Symposium on Dosimetry in Radiotherapy* (IAEA, Vienna, 1988), Vol 1, pp. 303–312.
- ³⁵E. Storm and H. I. Israel, "Photon cross sections from 1 keV to 100 MeV for elements $Z=1$ to $Z=100$," *At. Data Nucl. Data Tables* **7**, 565–681 (1970).
- ³⁶M. J. Berger and J. H. Hubbell, "XCOM: Photon cross sections on a personal computer," National Institute of Standards Technology Report No. NBSIR87-3597, 1987.
- ³⁷M. J. Berger, J. H. Hubbell, S. M. Seltzer, J. S. Coursey, and D. S. Zucker, "XCOM: Photon cross section database (version 1.2)," NIST Report, 1999, see <http://physics.nist.gov/xcom>.